

Cite this: *J. Mater. Chem. B*, 2019,
7, 2855Optical stereolithography of antifouling
zwitterionic hydrogels†Wenyang Pan,^{id}^a Thomas J. Wallin,^{id}^a Jérémy Odent,^{id}^a Mighten C. Yip,^{bc}
Bobak Mosadegh,^{bc} Robert F. Shepherd^{id}^d and Emmanuel P. Giannelis^{*a}

This paper reports the rapid 3D printing of tough (toughness, U_T , up to 141.6 kJ m⁻³), highly solvated ($\phi^{\text{water}} \sim 60$ v/o), and antifouling hybrid hydrogels for potential uses in biomedical, smart materials, and sensor applications, using a zwitterionic photochemistry compatible with stereolithography (SLA). A Design of Experiments (DOE) framework was used for systematically investigating the multivariate photochemistry of SLA generally and, specifically, to determine an aqueous SLA system with an additional zwitterionic acrylate, which significantly increases the gelation rate, and the resilience of the resulting hybrid hydrogels relative to an equivalent non-ionic polyacrylamide hydrogel. Specifically, the resulting zwitterionic hybrid hydrogels (Z-gels) can be tuned over a large range of ultimate strains, ca. $0.5 < \gamma_{\text{ult}} < 5.0$, and elastic moduli, ca. $10 < E < 1000$ kPa, while also demonstrating a high resilience under cyclic tensile loading. Importantly, unlike traditional chemistry, increasing the elastic modulus of the Z-gels does not necessarily reduce the ultimate strain. Moreover, the Z-gels can be rapidly printed using a desktop commercial SLA 3D printer, with relatively low photoirradiation dosages of visible light (135 to 675 mJ cm⁻² per 50–100 μm layer). Compared with the counterpart polyacrylamide hydrogels, the Z-gels have greater antifouling properties and exhibit 58.2% less absorption of bovine serum albumin.

Received 8th February 2019,
Accepted 21st March 2019

DOI: 10.1039/c9tb00278b

rsc.li/materials-b

Introduction

Hydrogels are percolated networks of hydrophilic polymers and are of considerable interest as smart biomaterials. These systems can possess mechanical properties similar to natural tissues (with elastic modulus ranging from 1 kPa $< E < 10$ MPa) and, in the case of acrylates (for example), are easily tuned for specific chemical responses (*e.g.*, swelling with physiological solutions necessary to promote cellular activity and growth).^{1,2} It is common to find these networks molded for numerous biomedical applications including DNA electrophoresis, drug delivery implants, biocompatible sensors and engineered tissues.³ Many next-generation uses of these materials (as actuators, smart stimuli-responsive materials, or implantable scaffolds) require more complex, three-dimensional patterning than molding affords,^{4,5} while still maintaining the properties that allow the hydrogels to be 3D printed.

Projection stereolithography (p-SLA) is a 3D printing strategy that selectively creates a desired structure layer-by-layer out of a

liquid pre-gel solution under exposure to patterned light (Fig. 1A). Unlike other 3D printing approaches, the spatial localization of the photopolymerization during SLA allows one to construct complex large-scale (tens of cm) objects of near arbitrary geometry with micron-scale resolution.⁶ Recently, high throughput SLA *via* continuous liquid interface production (CLIP) has further expanded the application space to include mass production by drastically reducing the fabrication times.⁷ The mechanical simplicity of p-SLA and CLIP (*i.e.*, one degree of freedom motion control), as well as the vat polymerization process it uses, makes this technique highly amenable to innovative photochemistry for functional materials.

In general, an ideal p-SLA compatible material is a low apparent viscosity (normally, $\mu_{\text{app}} < 5$ Pa s) liquid that flows quickly to form a new layer (patterning time < 15 s per layer) as it photopolymerizes into a self-supporting solid structure.^{8,9} Many hydrogels printed *via* SLA use concentrated solutions of low M_w acrylates, *e.g.* poly(ethylene glycol) diacrylate or acrylamide monomer (AAM), which quickly extend and crosslink during photo-exposure. The small mesh sizes of these gel networks, however, yield relatively brittle materials and narrow the utility of the resulting parts to prototype demonstrations.¹⁰ Applications such as tissue engineering, actuation, or chemical sensing, for example, would benefit from resilient, tough, and highly swellable hydrogels (*i.e.*, tunable crosslink density and polymer concentrations).^{11,12} While less time-sensitive casting and molding processes allow for low crosslink density in polymer

^a Materials Science & Engineering, Cornell University, Ithaca, NY 14853, USA.
E-mail: epg2@cornell.edu

^b Dalio Institute of Cardiovascular Imaging, New York-Presbyterian Hospital and Weill Cornell Medicine, New York, NY, 10065, USA

^c Department of Radiology, Weill Cornell Medicine, New York, NY, 10065, USA

^d Sibley School of Mechanical & Aerospace Engineering, Cornell University, Ithaca, NY 14853, USA

† Electronic supplementary information (ESI) available. See DOI: 10.1039/c9tb00278b

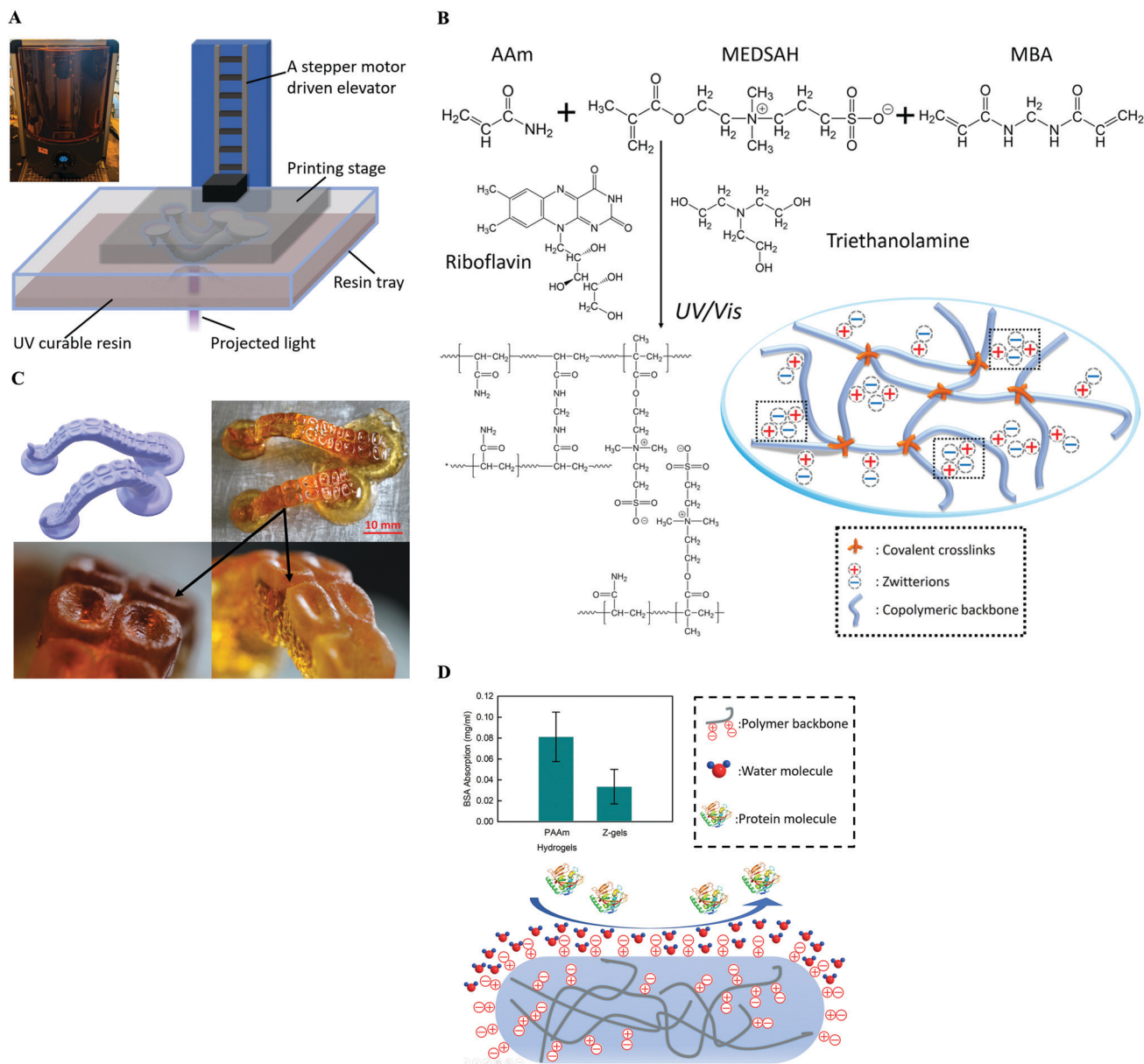


Fig. 1 Fabrication of the antifouling Z-gels through optical stereolithography: (A) schematic representation of the projection-stereolithography. (B) The zwitterionic hybrid hydrogel fabricated with acrylamide (AAm) and [2-(methacryloyloxy)ethyl]dimethyl-(3-sulfo)propyl)ammonium hydroxide (MEDSAH), having ionic crosslinks among the zwitterionic moieties and chemically crosslinked by MBA; riboflavin as the photoinitiator, and triethanolamine as the coinitiator. (C) The fast fabrication of octopus arms with 50 μm resolution, at the speed of 14 s per layer, through SLA. (D) Comparison of the BSA absorption of PAAm and the counterpart Z-gel with the same crosslink density. Lower figure shows the mechanism of improved antifouling property by using zwitterionic chemistry in the hydrogel resin.

gels (e.g., improving the ultimate strain, γ_{ult} , of the material), most SLA printers do not produce large enough photoirradiation dosages and thus require prohibitively long exposure times for the low crosslink density networks to gel.

One major strategy to improve the mechanical properties of the printed hydrogels is the use of double-network (DN) chemistries, which are typically composed of one heavily crosslinked (high E) polymer network and another interpenetrating, but lightly crosslinked (high γ_{ult}) network.^{13,14} Previously, research efforts on cast polyacrylamide (PAAm) DN hydrogels yielded high toughness and great ductility.^{13,14} The improved toughness results from the

energy dissipation of the highly crosslinked network fragmenting into small clusters during the mechanical deformation, while the flexible, loosely crosslinked network elastically deforms and uses the broken micro-scale primary network as physical entanglements.¹³ Unfortunately, this DN loses high toughness after the first loading cycle as the covalent crosslinks undergo permanent damage. The lack of recoverable mechanical performance restricts these DN hydrogels from use in practical devices that require repeated loadings.¹⁵ Therefore, many attempts have sought to replace the permanent sacrificial crosslinks with dynamic, recoverable bonds.^{15–20} Among the potential alternatives, the ionic bonds

offer significant promise owing to their rapid energy dissipation during Coulombic bond breaking-reforming.^{21,22} For example, Sun *et al.* reported a highly stretchable and tough alginate–PAAm hydrogel, which relies on the formation and breaking of calcium–alginate ionic clusters.^{23,24} This “unzipping” of the multivalent ionic clusters, instead of the rupture of covalent bonds, leads to a slow recovery of mechanical properties from the first deformation.²⁵

Here, we introduce a new approach based on an additional zwitterionic comonomer to the PAAm network for providing dynamic ionic bonds as the secondary network along the polymer backbone. This hybrid resin uses water-soluble riboflavin and triethanolamine (TEOHA) as the photoinitiator and coinitiator, respectively (Fig. 1B).^{26,27} Unlike the traditional DN hydrogels, this reaction requires only one step and allows for more direct and rapid SLA 3D printing. The zwitterionic acrylates possess both negative and positive charges, which endow the materials with a significant electrostatic attraction to water, low coefficient of friction, and extremely low bio-absorption that have resulted in their use as biocompatible surfaces or coatings, lubricants, and antifouling implantable devices.^{28–32} For example, implants made of zwitterionic hydrogels significantly reduce foreign-body reactions in mice.^{33,34} Compared with biocompatible poly(ethylene glycol) derivatives which are easily oxidized, zwitterionic materials impart higher resistance to oxidation and provide opportunities for long-term applications.³⁵ Additionally, riboflavin and TEOHA, unlike commercial photoinitiators such as Irgacure[®], have much lower cytotoxicity, initiate over lower energy visible wavelengths, and possess better solubility in aqueous solutions.³⁶ Due to these factors, we evaluated the potential of this hybrid hydrogel system (referred to as Z-gel henceforth) for biomedical applications by measuring their absorption of bovine serum albumin (BSA) as a metric for their antifouling properties.

With numerous interdependent variables involved in the structure–process–property relationship of the photopolymerized hydrogels (*e.g.*, monomer concentration, crosslink density, and photoirradiation dosage), we applied the design of experiments (DOE) methodology to quantify the influence of these factors on the patterning efficiency and the physicochemical properties of the resulting hydrogels. To provide quantitative measures for DOE, we used a photo-rheometer and photo-Differential Scanning Calorimetry (photo-DSC) to obtain *in situ* gelation, polymerization and rheological evolution data. Using the results of this DOE process, we identified appropriate precursor materials for the rapid 3D fabrication of resilient, tough and antifouling Z-gels.

Results and discussion

Photopolymerizable Z-gels contain intrinsic dynamic ionic bonds that improve toughness and resilience

For the rapid gelation of hydrogels with high tensile strength and large elastic strains, we copolymerize acrylamide (AAm) and zwitterionic acrylate, [2-(methacryloyloxy)ethyl] dimethyl-(3-sulfopropyl) ammonium hydroxide (MEDSAH), using *N,N'*-methylene bis(acrylamide) (MBA) as the multi-functional crosslinker (Fig. 1B). MEDSAH, due to its strongly ionizable sulfonate groups,

easily dissolves within a wide pH range in an aqueous solution.^{37,38} The ionic interactions, which arise between the anionic sulfonate groups and cationic quaternary amine groups from the neighboring zwitterionic moieties, produce additional electrostatic crosslinks that lead to resilient and tough hydrogels.

In the preliminary experiments, we have applied different MEDSAH to AAm weight ratios (from 0 to 100%) in the hybrid resins. Owing to the acidity of MEDSAH, more than 50 wt% MEDSAH led to acidic resins, in which more TEOHA needs to be used to maintain the resins in the reasonable pH range (neutral to slightly basic) for the riboflavin photochemistry. While using the same contents of riboflavin and TEOHA, gelation performance peaked when the hybrid resins contained ~50 wt% MEDSAH (equivalent to ~20% in molar ratio). In addition, the MEDSAH has a much higher molecular weight than AAm (279 Da *vs.* 71 Da). During the photo-polymerization, bulky pendant groups (*e.g.*, large zwitterionic moieties from MEDSAH) might sterically hinder the formation of high M_w polymers. Similar results have been reported previously.³⁹ In GPC measurements, we did observe higher molecular weight (M_w : 881.7 kDa *vs.* 391.3 kDa) of the non-crosslinked photopolymerized PAAm than that of the non-crosslinked Z-gel (monomers ratio ~50 : 50, wt/wt).

Therefore, to identify an appropriate SLA material, we reduced the number of potential experiments to a tractable amount by fixing the weight ratio of AAm to MEDSAH as 50 : 50 (molar ratio ~80 : 20) in this study. This ratio is similar to that of previously published ionomers, which normally have up to 15–20 mol% ionic species.⁴⁰

Based on the photo-rheological results, introducing MEDSAH into AAm solutions significantly improves the gelation rate, which is indicated by the more rapid rise of the G' (Fig. 2A and Fig. S1, ESI[†]). To minimize the reduction of the elastic strain regime from the addition of covalent crosslinker, we kept the MBA content low ($C_{MBA} \sim 0.011$ M) in both pre-gel solutions. Additionally, according to the multiple combinations of formulation composition and photoirradiation dosage based on the DOE, the Z-gels achieve significantly higher G' and G'' over the counterpart PAAm hydrogels (270 and 1361 times higher, respectively). These observations indicate that adding the dynamic ionic network significantly improves the gelling rate of the hydrogels, which is critical for the SLA fabrication.

Unlike conventional SLA solutions, in the Z-gel formulations, the rapid gelation and increase in G' does not correspond to a reduction in extensibility. To quantify our control over the mechanical properties of the Z-gels, we performed tensile tests (Fig. 2B). The results show that the Z-gels can be tuned to a wide range of elastic moduli ($10 < E < 1000$ kPa) and high ultimate strains ($0.5 < \gamma_{ult} < 5.0$), depending on the composition and photoirradiation dosage (I). By comparison, the same photoirradiation dosages applied to counterpart AAm solutions yield hydrogels that are too weak to load onto the tensile testing machine (Fig. 2C). This difference in tensile mechanical performance is easily inferred from the photo-rheological measurements (Fig. 2A).

Another major advantage of ionic crosslinks over the sacrificial covalent crosslinks is the ability to provide significant recoverable

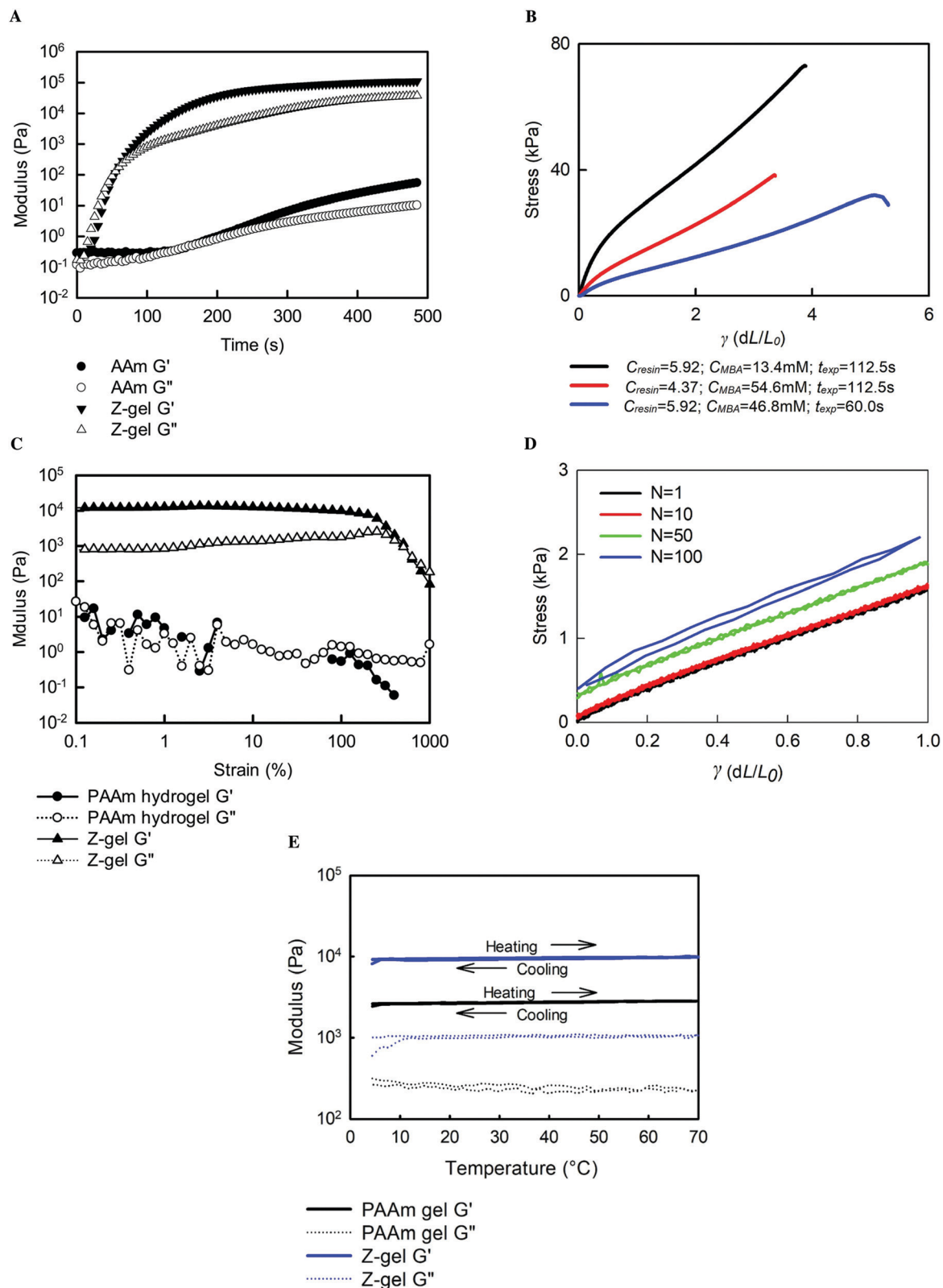


Fig. 2 Mechanical properties of the Z-gel. (A) The measurements of G' and G'' of the Z-gel during the photopolymerization, in comparison to the molar equivalent AAm hydrogels, respectively. (B) Ultimate strain (γ_{ult}) of the Z-gels with different monomer content (C_{resin}), crosslink density (C_{MBA}) and photoirradiation dosages (represented by t_{exp} under Omnicure 1500). (C) Significant improvement in the stiffness of the Z-gel over the PAAm hydrogel has been observed in typical strain sweep rheological tests. Both the Z-gel and PAAm hydrogels used in this measurement have equivalent resin composition ($C_{resin} = 4.374$, $C_{MBA} = 1.5$ mol%) and were exposed for the same amount of time ($t_{exp} = 112.5$ s). (D) Cyclic tensile tests of the Z-gel for 100 cycles. The dog bone shaped Z-gel was stretched to tensile strain ($\gamma = 1$) at the speed of 0.1 per min. (E) The heating-cooling cycle of temperature sweep rheological tests of as-prepared PAAm hydrogel and Z-gels. Both the Z-gel and PAAm hydrogels (same crosslink density) were cast in the PDMS mold and exposed under Omnicure 1500 until cured.

elastic deformation under tension. In our study, the Z-gel survived numerous loadings ($N = 100$, strain $\gamma = 1$) demonstrating high resilience and toughness. It is worth noting that the stress-strain curves shift upwards in later cycles, due to the incorporation of residual stresses resulting from evaporative water loss during the 12 hours of measurement (Fig. 2D). We attribute this outstanding resilience to the dynamic electrostatic interactions that dissipate the deformation energy primarily through the relaxation of the polymer chains *via* spontaneous breaking-reattaching of ionic bonds between adjacent sulfonate-quaternary amine groups. Previous research by Guo *et al.* and Long *et al.* also proved that stress relaxation in recoverable DN hydrogels is dominated by the breaking and reattaching of reversible dynamic bonds, instead of the permanent rupture of the covalent crosslinks.^{41,42}

In addition to the mechanical testing and oscillatory rheology measurements, we evaluated the thermal stability of the as-prepared hydrogels using oscillatory rheology over a temperature sweep between 4 and 70 °C (Fig. 2E). The evolution of moduli (G' and G'') from this heating-cooling cycle showed that both the Z-gel and the counterpart PAAm hydrogel were stable over a broad range of temperatures.

Our hybrid zwitterionic hydrogel system is also quite distinct from the alginate-AAm ionic hydrogels, where the type and valence of exogenous cations play a critical role in mechanical performance.⁴³ For example, the addition of multivalent cations (*e.g.*, Ca^{2+} or Al^{3+}) is required for toughening the alginate-AAm hydrogels, while the gels supplemented by Na^+ show only minimal improved toughness.²³ By attaching the ionic groups to the polymeric backbone, the Z-gel's ionic interactions remain

largely unaffected by the exogenous salts that will be encountered in physiologically relevant environments. Thus, the photopolymerization kinetics (*e.g.*, gelation speed and moduli) did not change when adding equivalent molar content of sodium (monovalent) or even calcium (divalent) chloride salts to the zwitterionic monomers (Fig. S2, ESI[†]). Therefore, we attribute the enhanced moduli, ultimate strain and the rapid gelling performance shown in the Z-gels to the interactions among the zwitterionic neighboring moieties.

DOE optimization of the Z-gels for SLA 3D printing

Due to the complexity of the system, multiple factors simultaneously affect the efficiency and rate of photopolymerization, as well as the properties of the resulting hydrogels. Firstly, fine-tuning of the riboflavin and TEOHA is critical because the rate of free radical polymerization depends on their combined and relative amounts in aqueous solutions.²⁶ Neutral to basic conditions in the pre-gel solutions are reported to facilitate the formation of the riboflavin-TEOHA radical pairs, which then initiates the free radical polymerization.⁴⁴ Moreover, the monomer content (C_{resin}), crosslink density (C_{MBA}), and degree of polymerization impact the mechanical properties of the hydrogels. Consequently, we tailored these parameters with an eye towards increased printing speed and optimum properties of elastomeric hydrogels. With an intractable amount of chemical compositions and external variables to control, we used the DOE methodology to narrow the design space and perform a thorough investigation of the SLA system.

First, we investigated the ratio and total amount of photo-initiator and coinitiator within a simplest AAm pre-gel solution

Table 1 The combinations of riboflavin and TEOHA contents (based on mixture design), and their effects on the gelation speed of PAAm hydrogels (based on the photo-rheological measurements). Sampling interval was 0.5 s. The pre-gel solutions of AAm contained 5.9 M AAm and ~2.4 mol% MBA

Standard order	Riboflavin (μL)	Triethanolamine (μL)	When $G' > 1$ Pa	When $G' > 10$ Pa	When $G' > 10^2$ Pa	When $G' > 10^3$ Pa	When $G' > 10^4$ Pa
1	45	5	24	39.5	72	112	165
2	5	45	17.5	25	37	105	116.5
3	25	25	19	29	46.5	66.5	132.5
4	35	15	22	35	60	89	131.5
5	15	35	18.5	27.5	39	55	91
6	90	10	23.5	34.5	65.5	113.5	166.5
7	10	90	18.5	26.5	38.5	53.5	83.5
8	50	50	22	32.5	52	76	113.5
9	70	30	20.5	30.5	58.5	102.5	158
10	30	70	18.5	27	42.5	64.5	127.5
11	180	20	26	38.5	96.5	198.5	1000
12	20	180	20	28.5	41.5	54	78
13	100	100	22	31.5	61	91.5	139
14	140	60	35	48	77	116	188
15	60	140	34	48.5	70.5	92	129
16	450	50	1000 ^a	1000	1000	1000	1000
17	50	450	60	78.5	108.5	150	222
18	250	250	1000	1000	1000	1000	1000
19	350	150	1000	1000	1000	1000	1000
20	150	350	211	272	1000	1000	1000
21	900	100	1000	1000	1000	1000	1000
22	100	900	1000	1000	1000	1000	1000
23	500	500	1000	1000	1000	1000	1000
24	700	300	1000	1000	1000	1000	1000
25	300	700	1000	1000	1000	1000	1000

^a The gelation time was assigned as 1000 s when the hydrogel failed to reach a certain level of G' during the photo-rheological tests which last for 500 s.

containing a fixed amount of MBA, aiming to identify combinations that enable rapid photopolymerization (Table 1). We found that with different combinations of riboflavin and TEOHA, the gel point varied broadly from 25 s to 300 s when exposed to a low photoirradiation dosage (Omnicure Series 1500, photoirradiation density $\sim 6.20 \text{ mW cm}^{-2}$, Lumen dynamic) (Fig. 3A). From the results, we selected $7.1 \mu\text{L}$ of 1 mg mL^{-1} riboflavin as

an efficient photoinitiator dosage and $71.4 \mu\text{L}$ of 300 mg mL^{-1} TEOHA, per gram of monomers for the rapid gelling, and maintaining the pre-gel solutions in the appropriate pH range, even with the addition of an acidic MEDSAH comonomer.

After fixing the photoinitiator and sensitizer concentrations, we used multi-factorial and multi-level response surface designs in the DOE to investigate the effects of monomer content,

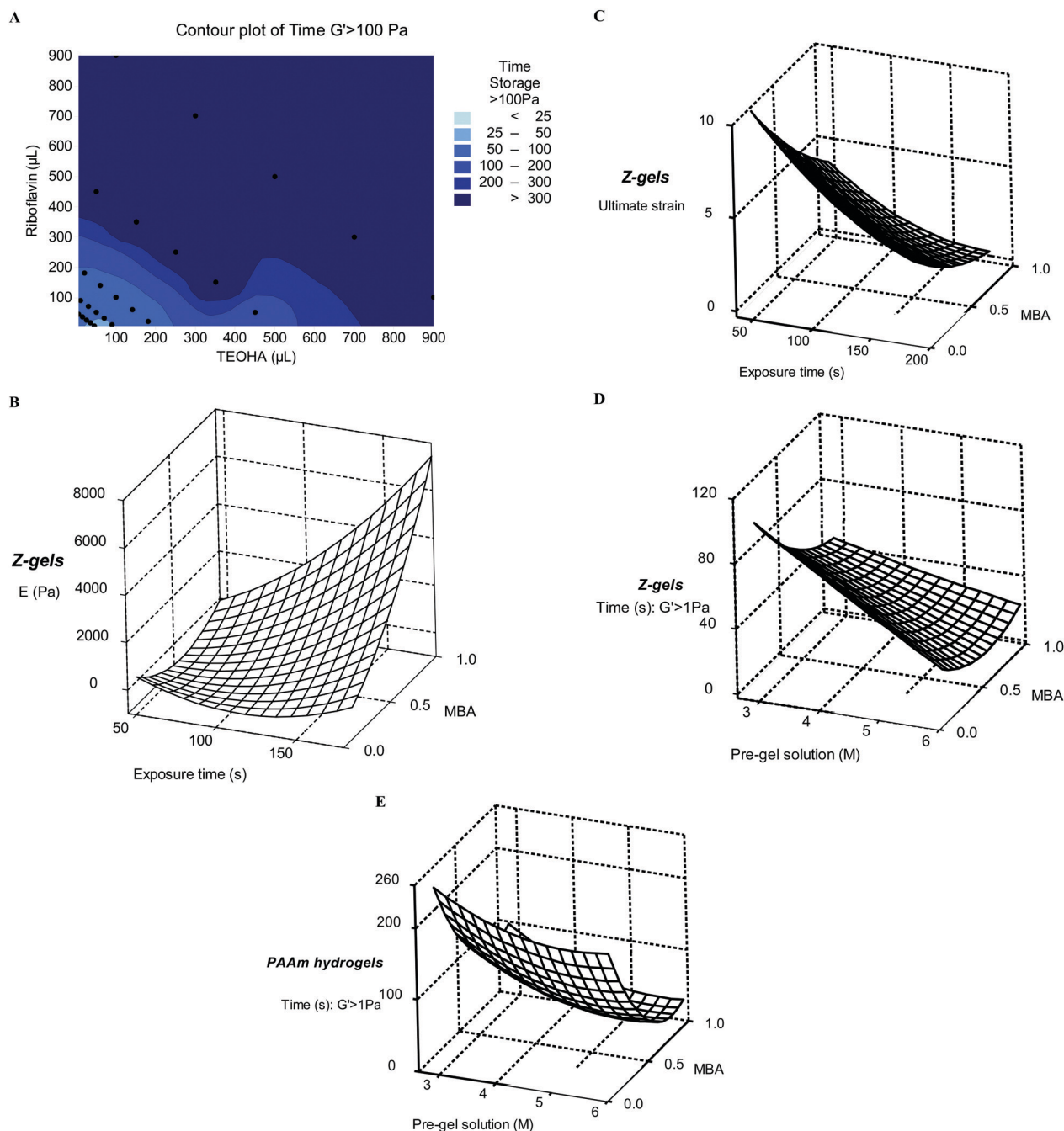


Fig. 3 Investigation and modeling of the Z-gel system. (A) The contour map of time when $G' > 100 \text{ Pa}$ vs. the riboflavin and TEOHA ratio, based on the mixture design. Lighter colors indicate faster gelation. (B) The response surface plot of the elastic modulus E (kPa) against the monomer content and exposure time. The contents of MBA as chemical crosslinker in the DOE models were represented by their relative ratio to monomer contents (the value 1 equals to $1/42 \text{ mol}$ of monomer content, which was predetermined as the upper limit for MBA). (C) The response surface plot of the ultimate strain γ_{ult} against the MBA content and exposure time based on Box–Behnken design. (D) The response surface plot of time when $G' > 1 \text{ Pa}$ for the Z-gels. (E) The response surface plot of time when $G' > 1 \text{ Pa}$ for the PAAm hydrogels, which are more dependent on the crosslink density, compared with the monomer content.

Table 2 Box–Behnken design of a 3-factor (C_{resin} , C_{MBA} and t_{exp}) experiment and the corresponding responses (G' , G'' , ultimate strain, Young's modulus and swelling ratio). The as prepared Z-gels were subjected to strain sweep rheological tests (G' and G'' , data were taken when the strain was 10% at the fixed angular frequency at 1 rad s^{-1})

Standard order	t_{exp} (s)	C_{MBA}^a	C_{resin} (M)	G' (Pa)	G'' (Pa)	Ultimate strain (%)	Young's modulus (kPa)	Swelling ratio q
1	45	0.1	4.374	280	335	1000.0 ^b	1 ^b	10 ^b
2	180	0.1	4.374	2610	1590	357.9	228	3.96
3	45	1	4.374	14800	3610	381.8	17	1.48
4	180	1	4.374	989	2250	67.2	7599	1.68
5	45	0.55	2.824	1	1.15	1000.0	1	10
6	180	0.55	2.824	783	341	239.8	93	1.47
7	45	0.55	5.924	2670	850	368.3	51	2.03
8	180	0.55	5.924	3480	1390	53.8	7522	2.40
9	112.5	0.1	2.824	1	1.15	1000.0	1	10
10	112.5	1	2.824	879	224	164.0	26	1.19
11	112.5	0.1	5.924	15 700	4690	328.0	611	3.29
12	112.5	1	5.924	116 000	20 200	36.0	6992	1.61
13	112.5	0.55	4.374	8940	1690	309.1	107	2.06
14	112.5	0.55	4.374	6250	914	309.1	107	1.96
15	112.5	0.55	4.374	9910	1790	309.1	107	2.02

^a C_{MBA} as a chemical crosslinker was represented by its relative ratio to C_{resin} (the value 1 equals 1/42 mol of C_{resin} , which was predetermined as the upper limit for C_{MBA}). ^b The ultimate strain (%), Young's modulus and swelling ratio were assigned as 1000.0%, 1 kPa and 10, respectively, for hydrogels that were too soft to use in tensile tests.

crosslink density and photoirradiation dosage on the gelation and the resulting mechanical performance (Table 2). We selected the storage modulus (G') of the gelling network, tensile elastic modulus (E) of the resultant elastomer, and ultimate strain (γ_{ult}) as the key mechanical metrics. Unsurprisingly, the corresponding models show that higher monomer content, crosslink density, or photoirradiation dosage (represented as the exposure time) results in a stiffer but less stretchable hydrogel (Fig. 3B, C, Table 2 and Tables S1, S2, ESI†). To gain deeper insight, we used photoirradiation dosage as the tuning parameter to understand what pre-gel solution compositions could produce desirable mechanical properties at low dosages, required by the fast SLA process. Choosing relatively low photoirradiation dosage ($I \sim 372 \text{ mJ cm}^{-2}$) as our objective, led to a formulation with excellent ultimate strain ($\gamma_{\text{ult}} = 4.76$, at an $E \sim 246 \text{ kPa}$).

We then used DOE to investigate the swelling behavior of the Z-gels (swelling ratio = W_s/W_0). While some applications benefit from hydrogel swelling (e.g., osmotic actuation),¹⁸ other applications, e.g., implantable biomedical devices, prefer a low q . We soaked all the as-prepared Z-gels in 37 °C deionized water for 48 hours until the absorbed weight plateaued. We clearly observed the inverse correlation of q versus C_{resin} , C_{MBA} , and t_{exp} (Table 2 and Fig. S3, ESI†), among which the crosslink density (C_{MBA}) was slightly more influenced followed by the photoirradiation dosage and then C_{resin} . Among all combinations in DOE, the formulation with $C_{\text{resin}} = 4.37 \text{ M}$, $C_{\text{MBA}} = 0.024 \text{ M}$ MBA and $I = 279 \text{ mJ cm}^{-2}$ has pretty good ultimate strain ($\gamma_{\text{ult}} = 3.81$) and relatively low swelling ratio ($q = 1.48$).

While the Z-gels that we have so-far reported show tunable mechanical properties and swelling, we have used DOE to optimize t_{gel} , which we defined as when $G' > 1 \text{ Pa}$, of AAm and zwitterionic formulations to be more compatible with rapid layer fabrication in SLA, using photo-rheological results. Consistent with expectations, we found that increasing C_{resin} or C_{MBA} decreases the photoirradiation necessary for gelation (Fig. 3D, E, Table 3 and Tables S3, S4, ESI†). For example, when C_{resin} is fixed, increased

Table 3 Central composite design (CCD) of 2-factor (C_{resin} and C_{MBA}) photo-rheological tests and the corresponding response (time when $G' > 1 \text{ Pa}$) to represent the initiation of gelation. All samples were subjected to 500 s exposure from Omnicure 1500

	C_{resin} (M)	C_{MBA}^a	Z-gel solutions when $G' > 1 \text{ Pa}$ (s)	AAM solutions when $G' > 1 \text{ Pa}$ (s)
1	2.824	0.1	102.5	239.0
2	5.924	0.1	26.5	198.0
3	2.824	1	46.0	88.5
4	5.924	1	19.0	33.5
5	2.824	0.55	59.0	129.5
6	5.924	0.55	19.5	43.5
7	4.374	0.1	66.0	201.5
8	4.374	1	33.5	44.0
9	4.374	0.55	36.0	56.5
10	4.374	0.55	36.0	56.5
11	4.374	0.55	36.0	56.5
12	4.374	0.55	36.0	56.5
13	4.374	0.55	36.0	56.5

^a C_{MBA} was represented by their relative ratio to C_{resin} (the value 1 equals to 1/42 mol of C_{resin} , which was predetermined as the upper limit for MBA).

C_{MBA} leads to a faster polymerization (Fig. S4A, ESI†). On the other hand, with a fixed C_{MBA} , more concentrated pre-gel solutions gel more rapidly (Fig. S4B, ESI†). Compared with AAm solutions (response surface shown in Fig. 3E), the zwitterionic formulations (Fig. 3D) exhibited a markedly faster gelation rate in both the initiation (50% faster than AAm, on average) and maturation of gelation (17% faster), represented by the time of G' reaching 1 Pa at the early stage and to more than 90% of the final plateau G' , respectively.

Using the results from DOE, we demonstrated the 3D printing of Z-gels with complex 3D structures, using projection SLA (Fig. 1A). Based on the composition and their corresponding gel time, I varied from 135 to 675 mJ cm^{-2} per layer in the desktop SLA (Autodesk Ember) printer, which corresponds to 6 to 30 s of exposure. These photoirradiation dosages are comparable with previous research using 2,4,6-trimethylbenzoyl-diphenylphosphine

oxide (TPO) nanoparticles as a water dispersible photoinitiator, which required complicated modifications of TPO to overcome its insolubility in aqueous solutions.⁴⁵ Therefore, the riboflavin and TEOHA initiation chemistry we used is advantageous due to its simplicity, better water solubility, and great biocompatibility.³⁶

To demonstrate the capability of our SLA compatible Z-gels, we selected one zwitterionic solution ($C_{\text{resin}} = 4.37 \text{ M}$) with medium crosslink density ($C_{\text{MBA}} = 1.5 \text{ mol\%}$) to print soft octopus arms. The 3D fabrication of this hydrogel was performed at a rate of 14 s ($\Gamma \sim 315 \text{ mJ cm}^{-2}$) per layer at a high resolution ($50 \mu\text{m}$ thickness each layer) (Fig. 1C). A demonstration of high-resolution SLA (represented by a rose) is shown in a supporting video (Video S1, ESI†).

Z-gel photopolymerization kinetics

We also observed a different gelation pattern of the Z-gels compared to the PAAm gels. The gelation rate of the AAm resins relies more on the crosslink density represented by its steeper slope along the axis of C_{MBA} , compared with that of C_{resin} (Fig. 3E). The zwitterionic formulations, in which C_{resin} has an effect on the strength of ionic interactions, exhibit a stronger response to variations in C_{resin} on the response surface than that of C_{MBA} (Fig. 3D). This distinction clearly indicates that the zwitterionic comonomer is critical to the fast gelation behavior of the Z-gels (Fig. 2A). This finding is especially important as methacrylate groups of the MEDSAH are theoretically considered less reactive during the polymerization than the acrylate groups of AAm, owing to the higher stability of the tertiary radicals formed on the MEDSAH than the secondary radicals formed on AAm. MEDSAH, however, is ionized and negatively charged in the aqueous solution over a large pH range ($2 < \text{pH} < 10$). Therefore, in the pre-gel solutions, the zwitterions are assumed to present as the acidic counter-ions to the basic TEOHA.^{44,46} As a result, the initiation in the Z-gel formulations might start from the zwitterions that are ionically interacting with TEOHA.

We tested this assumption on initiation by comparing the photo-DSC patterns of zwitterionic and AAm formulations. The zwitterionic solution showed two distinct but much narrower heat flow peaks, indicating a more rapid polymerization and a preference for a certain monomer. The AAm solution, however, showed only a broader single peak that indicates a slower polymerization (Fig. S5, ESI†). Moreover, it was previously proposed that stronger ionic interactions, like those found in the zwitterionic formulations, cause the growing polymer chains to coil more so that the pendant acrylates are more easily and advantageously exposed to other free radical species.⁴⁷

We further characterized the Z-gel by a $400 \text{ MHz } ^1\text{H NMR}$ spectrum which showed the copolymerization of the AAm and MEDSAH (Fig. S6, ESI†). Thermal analyses were performed on both as prepared and freeze-dried hydrogels. The DSC measurement of the dried Z-gel (Fig. S7A, ESI†) indicated that the photopolymerized network behaves like a random copolymer with only one glass transition at $\sim 140^\circ\text{C}$. On the other hand, DSC of the as prepared Z-gel showed a transition at $\sim 150^\circ\text{C}$, which was previously reported as the dehydration temperature⁴⁸ (Fig. 4A). Interestingly, the dehydration temperature of the counterpart PAAm hydrogel was $\sim 120^\circ\text{C}$. We attribute this

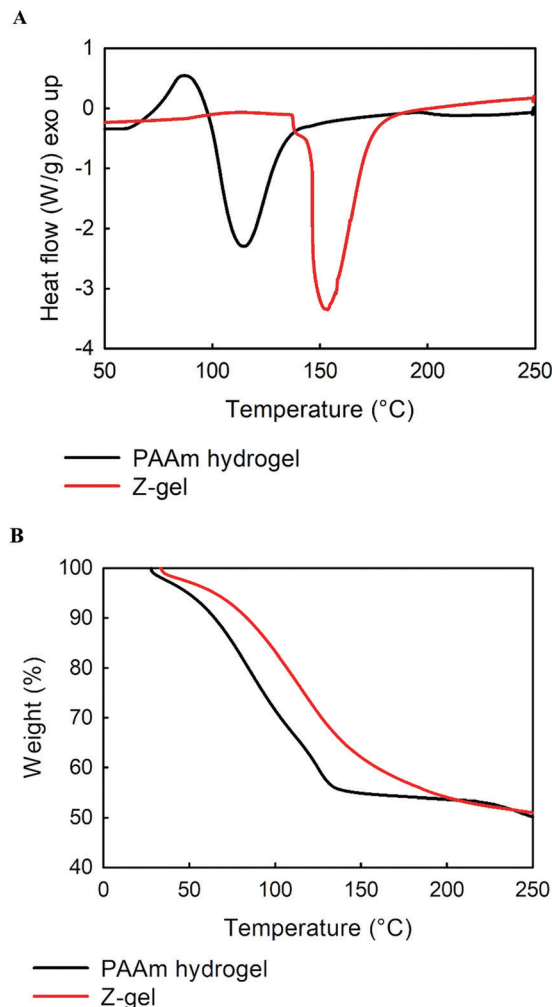


Fig. 4 Thermal properties of the as-prepared Z-gel and PAAm hydrogel. (A) DSC measurement of the as-prepared Z-gel and counterpart PAAm hydrogel. (B) TGA of the as-prepared Z-gel and PAAm hydrogel.

30°C difference to a greater hydrophilicity of the Z-gels, which leads to stronger water affinity.

From TGA, the as-prepared Z-gel was more thermally stable than the PAAm hydrogel by presenting smaller weight loss before 200°C , probably owing to the additional ionic crosslinks (Fig. 4B). The dried Z-gel represented similar behavior with the onset degradation temperature of $\sim 250^\circ\text{C}$, which is about 30°C higher than that of the dried PAAm (Fig. S7B, ESI†).

Antifouling tests

We compare the antifouling performance of the zwitterionic and PAAm hydrogels based on a protein absorption measurement using bovine serum albumin (BSA) as the model protein. After six hours of soaking in the BSA solution, the Z-gels absorbed significantly less BSA (58.2%) than the counterpart PAAm hydrogels ($81.2 \mu\text{g mL}^{-1}$ BSA absorption of PAAm hydrogels *versus* $33.5 \mu\text{g mL}^{-1}$ of the corresponding Z-gels). This behavior agrees with previously reported research which applied zwitterionic polymers.^{49–51} We attribute the significantly improved antifouling

behavior to the super hydrophilicity of the zwitterionic moieties, which absorb excessive layers of water molecules on the hydrogel surface and thus exhibit strong repulsive forces against surrounding protein molecules (Fig. 1D).⁴⁹ The antifouling performance is believed to be positively correlated to the surface density of the zwitterionic groups.⁵²

Conclusions

3D printing *via* projection stereolithography is a promising approach for the construction of complex soft material systems for future applications in smart materials, soft actuators and sensors, and biomedical devices. The limited availability of hydrogel materials, however, restricts progress in many of these areas. In this paper, we report and characterize a novel SLA platform that integrates zwitterionic chemistry and a simple but efficient aqueous photoinitiation system. The introduction of the zwitterionic comonomer into acrylamide has significantly improved the patterning rate of the SLA system and overcome the weakness of the traditional DN hydrogels, thereby enabling the rapid fabrication of elastic and tough hydrogels. Furthermore, we employed DOE methodology to perform a systematic optimization and investigation of the gelation rate, swelling behavior, and mechanical properties and used the results to guide the hydrogel formulations for optimal properties.

We found that the copolymerization of the MEDSAH and AAm, using the biocompatible photochemistry of riboflavin and TEOHA, produced hybrid hydrogels with significantly improved antifouling properties, which could make these materials well suited for 3D printed biomedical devices. Furthermore, our platform is versatile and can be easily modified for specific applications and desirable properties. For example, instead of using AAm, thermally responsive hydrogel materials such as *N*-isopropylacrylamide could be used as implantable and targeted drug delivery devices to broaden the intended application space of these materials.

Conflicts of interest

The authors declare no conflict of interest.

Acknowledgements

This work is supported by the Air Force Office of Scientific Research, Contract: FA9550-18-1-0243. We also acknowledge the use of the Cornell Center for Materials Research Shared Facilities which are supported through the NSF MRSEC program (DMR-1719875).

References

- 1 K. Y. Lee and D. J. Mooney, Hydrogels for tissue engineering, *Chem. Rev.*, 2001, **101**, 1869–1880.
- 2 A. S. Hoffman, Hydrogels for biomedical applications, *Adv. Drug Delivery Rev.*, 2002, **54**, 3–12.
- 3 M. Matsusaki, H. Yoshida and M. Akashi, The construction of 3D-engineered tissues composed of cells and extracellular matrices by hydrogel template approach, *Biomaterials*, 2007, **28**, 2729–2737.
- 4 F. P. Melchels, J. Feijen and D. W. Grijpma, A review on stereolithography and its applications in biomedical engineering, *Biomaterials*, 2010, **31**, 6121–6130.
- 5 I. Willner, *Stimuli-Controlled Hydrogels and Their Applications*, ACS Publications, 2017.
- 6 S. Maruo and K. Ikuta, Submicron stereolithography for the production of freely movable mechanisms by using single-photon polymerization, *Sens. Actuators, A*, 2002, **100**, 70–76.
- 7 J. R. Tumbleston, D. Shirvanyants, N. Ermoshkin, R. Januszewicz, A. R. Johnson and D. Kelly, *et al.*, Continuous liquid interface production of 3D objects, *Science*, 2015, **347**, 1349–1352.
- 8 T. Chartier, M. Ferrato and J. Baumard, Debinding of ceramics: a review, *Ceram. Acta*, 1994, **6**, 17–27.
- 9 T. Chartier, C. Hinczewski and S. Corbel, UV curable systems for tape casting, *J. Eur. Ceram. Soc.*, 1999, **19**, 67–74.
- 10 J. Dulieu-Barton and M. Fulton, Mechanical properties of a typical stereolithography resin, *Strain*, 2000, **36**, 81–87.
- 11 J. L. Drury and D. J. Mooney, Hydrogels for tissue engineering: scaffold design variables and applications, *Biomaterials*, 2003, **24**, 4337–4351.
- 12 E. M. White, J. Yatvin, J. B. Grubbs, J. A. Bilbrey and J. Locklin, Advances in smart materials: stimuli-responsive hydrogel thin films, *J. Polym. Sci., Part B: Polym. Phys.*, 2013, **51**, 1084–1099.
- 13 J. P. Gong, Why are double network hydrogels so tough?, *Soft Matter*, 2010, **6**, 2583–2590.
- 14 J. P. Gong, Y. Katsuyama, T. Kurokawa and Y. Osada, Double-network hydrogels with extremely high mechanical strength, *Adv. Mater.*, 2003, **15**, 1155–1158.
- 15 J.-Y. Sun, X. Zhao, W. R. Illeperuma, O. Chaudhuri, K. H. Oh and D. J. Mooney, *et al.*, Highly stretchable and tough hydrogels, *Nature*, 2012, **489**, 133–136.
- 16 H. Yuk, T. Zhang, S. Lin, G. A. Parada and X. Zhao, Tough bonding of hydrogels to diverse non-porous surfaces, *Nat. Mater.*, 2016, **15**, 190–196.
- 17 X. Zhao, Multi-scale multi-mechanism design of tough hydrogels: building dissipation into stretchy networks, *Soft Matter*, 2014, **10**, 672–687.
- 18 J. Odent, T. J. Wallin, W. Pan, K. Kruemplestaedter, R. F. Shepherd and E. P. Giannelis, Highly Elastic, Transparent, and Conductive 3D-Printed Ionic Composite Hydrogels, *Adv. Funct. Mater.*, 2017, **27**, 1701807.
- 19 S. E. Bakarich, G. C. Pidcock, P. Balding, L. Stevens and P. Calvert, Recovery from applied strain in interpenetrating polymer network hydrogels with ionic and covalent cross-links, *Soft Matter*, 2012, **8**, 9985–9988.
- 20 S. E. Bakarich, S. Beirne, G. G. Wallace and G. M. Spinks, Extrusion printing of ionic-covalent entanglement hydrogels with high toughness, *J. Mater. Chem. B*, 2013, **1**, 4939–4946.
- 21 C. W. Peak, J. J. Wilker and G. Schmidt, A review on tough and sticky hydrogels, *Colloid Polym. Sci.*, 2013, **291**, 2031–2047.
- 22 A. S. Hoffman, Hydrogels for biomedical applications, *Adv. Drug Delivery Rev.*, 2012, **64**, 18–23.
- 23 C. H. Yang, M. X. Wang, H. Haider, J. H. Yang, J.-Y. Sun and Y. M. Chen, *et al.*, Strengthening alginate/polyacrylamide

- hydrogels using various multivalent cations, *ACS Appl. Mater. Interfaces*, 2013, **5**, 10418–10422.
- 24 D. Şolpan, M. Torun and O. Güven, The usability of (sodium alginate/acrylamide) semi-interpenetrating polymer networks on removal of some textile dyes, *J. Appl. Polym. Sci.*, 2008, **108**, 3787–3795.
- 25 H. Kamata, Y. Akagi, Y. Kayasuga-Kariya, U.-I. Chung and T. Sakai, “Nonswellable” hydrogel without mechanical hysteresis, *Science*, 2014, **343**, 873–875.
- 26 S. Bertolotti, C. Previtali, A. Rufs and M. Encinas, Riboflavin/triethanolamine as photoinitiator system of vinyl polymerization. A mechanistic study by laser flash photolysis, *Macromolecules*, 1999, **32**, 2920–2924.
- 27 B. Orellana, A. Rufs, M. Encinas, C. Previtali and S. Bertolotti, The photoinitiation mechanism of vinyl polymerization by riboflavin/triethanolamine in aqueous medium, *Macromolecules*, 1999, **32**, 6570–6573.
- 28 G. Cheng, G. Li, H. Xue, S. Chen, J. D. Bryers and S. Jiang, Zwitterionic carboxybetaine polymer surfaces and their resistance to long-term biofilm formation, *Biomaterials*, 2009, **30**, 5234–5240.
- 29 M. Tanaka, K. Sato, E. Kitakami, S. Kobayashi, T. Hoshiba and K. Fukushima, Design of biocompatible and biodegradable polymers based on intermediate water concept, *Polym. J.*, 2015, **47**, 114–121.
- 30 M. T. Bernards, G. Cheng, Z. Zhang, S. Chen and S. Jiang, Nonfouling polymer brushes via surface-initiated, two-component atom transfer radical polymerization, *Macromolecules*, 2008, **41**, 4216–4219.
- 31 H. Nandivada, L. G. Villa-Diaz, K. S. O’Shea, G. D. Smith, P. H. Krebsbach and J. Lahann, Fabrication of synthetic polymer coatings and their use in feeder-free culture of human embryonic stem cells, *Nat. Protoc.*, 2011, **6**, 1037–1043.
- 32 A. O. Osaheni, E. B. Finkelstein, P. T. Mather and M. M. Blum, Synthesis and characterization of a zwitterionic hydrogel blend with low coefficient of friction, *Acta Biomater.*, 2016, **46**, 245–255.
- 33 L. Zhang, Z. Cao, T. Bai, L. Carr, J. R. Ella-Menye and C. Irvin, *et al.*, Zwitterionic hydrogels implanted in mice resist the foreign-body reaction, *Nat. Biotechnol.*, 2013, **31**, 553–556.
- 34 Z. Zhang, T. Chao, L. Liu, G. Cheng, B. D. Ratner and S. Jiang, Zwitterionic hydrogels: an in vivo implantation study, *J. Biomater. Sci., Polym. Ed.*, 2009, **20**, 1845–1859.
- 35 H. Yin, T. Akasaki, T. L. Sun, T. Nakajima, T. Kurokawa and T. Nonoyama, *et al.*, Double network hydrogels from poly-zwitterions: high mechanical strength and excellent anti-biofouling properties, *J. Mater. Chem. B*, 2013, **1**, 3685–3693.
- 36 A. K. Nguyen, S. D. Gittard, A. Koroleva, S. Schlie, A. Gaidukeviciute and B. N. Chichkov, *et al.*, Two-photon polymerization of polyethylene glycol diacrylate scaffolds with riboflavin and triethanolamine used as a water-soluble photoinitiator, *Regener. Med.*, 2013, **8**, 725–738.
- 37 A. J. Schmid, R. Schroeder, T. Eckert, A. Radulescu, A. Pich and W. Richtering, Synthesis and solution behaviour of stimuli-sensitive zwitterionic microgels, *Colloid Polym. Sci.*, 2015, **293**, 3305–3318.
- 38 M. Das, N. Sanson and E. Kumacheva, Zwitterionic poly (betaine-*n*-isopropylacrylamide) microgels: properties and applications, *Chem. Mater.*, 2008, **20**, 7157–7163.
- 39 M. Zhang, C. Shan, L. Liu, J. Liao, Q. Chen and M. Zhu, *et al.*, Facilitating anion transport in polyolefin-based anion exchange membranes via bulky side chains, *ACS Appl. Mater. Interfaces*, 2016, **8**, 23321–23330.
- 40 R. Varley, *Ionomers as self healing polymers. Self Healing Materials*, Springer, 2007, pp. 95–114.
- 41 J. Guo, R. Long, K. Mayumi and C.-Y. Hui, Mechanics of a Dual Cross-Link Gel with Dynamic Bonds: Steady State Kinetics and Large Deformation Effects, *Macromolecules*, 2016, **49**, 3497–3507.
- 42 R. Long, K. Mayumi, C. Creton, T. Narita and C.-Y. Hui, Rheology of a dual crosslink self-healing gel: theory and measurement using parallel-plate torsional rheometry, *J. Rheol.*, 2015, **59**, 643–665.
- 43 C. K. Kuo and P. X. Ma, Ionically crosslinked alginate hydrogels as scaffolds for tissue engineering: Part 1. Structure, gelation rate and mechanical properties, *Biomaterials*, 2001, **22**, 511–521.
- 44 M. Encinas, A. Rufs, S. Bertolotti and C. Previtali, Free radical polymerization photoinitiated by riboflavin/amines. Effect of the amine structure, *Macromolecules*, 2001, **34**, 2845–2847.
- 45 A. A. Pawar, G. Saada, I. Cooperstein, L. Larush, J. A. Jackman and S. R. Tabaei, *et al.*, High-performance 3D printing of hydrogels by water-dispersible photoinitiator nanoparticles, *Sci. Adv.*, 2016, **2**, e1501381.
- 46 L. Wu, J. Jasinski and S. Krishnan, Carboxybetaine, sulfobetaine, and cationic block copolymer coatings: a comparison of the surface properties and antibiofouling behavior, *J. Appl. Polym. Sci.*, 2012, **124**, 2154–2170.
- 47 K. Haraguchi, H.-J. Li, K. Matsuda, T. Takehisa and E. Elliott, Mechanism of forming organic/inorganic network structures during in-situ free-radical polymerization in PNIPAA-clay nanocomposite hydrogels, *Macromolecules*, 2005, **38**, 3482–3490.
- 48 R. Lalani and L. Liu, Synthesis, characterization, and electrospinning of zwitterionic poly (sulfobetaine methacrylate), *Polymer*, 2011, **52**, 5344–5354.
- 49 Y.-F. Zhao, L.-P. Zhu, Z. Yi, B.-K. Zhu and Y.-Y. Xu, Zwitterionic hydrogel thin films as antifouling surface layers of polyethersulfone ultrafiltration membranes anchored via reactive copolymer additive, *J. Membr. Sci.*, 2014, **470**, 148–158.
- 50 T. Xiang, C.-D. Luo, R. Wang, Z.-Y. Han, S.-D. Sun and C.-S. Zhao, Ionic-strength-sensitive polyethersulfone membrane with improved anti-fouling property modified by zwitterionic polymer via in situ cross-linked polymerization, *J. Membr. Sci.*, 2015, **476**, 234–242.
- 51 F. Razi, I. Sawada, Y. Ohmukai, T. Maruyama and H. Matsuyama, The improvement of antibiofouling efficiency of polyethersulfone membrane by functionalization with zwitterionic monomers, *J. Membr. Sci.*, 2012, **401**, 292–299.
- 52 C. Ma, H. Zhou, B. Wu and G. Zhang, Preparation of polyurethane with zwitterionic side chains and their protein resistance, *ACS Appl. Mater. Interfaces*, 2011, **3**, 455–461.